Available online at www.sciencedirect.com
SCIENCE DIRECT
Journal of Membrane Science 280 (2006) 867–875
journal of MEMBRANE SCIENCE
www.elsevier.com/locate/memsci

Synthesis and characterization of MCM-48 tubular membranes

O. de la Iglesia [a], M. Pedernera [b], R. Mallada [a], Z. Lin [c], J. Rocha [c], J. Coronas [a], J. Santamaría [a,*]

[a] *Departamento de Ingeniería Química y Tecnologías del Medio Ambiente, Universidad de Zaragoza, Spain*
[b] *Planta Piloto de Ingeniería Química, UNS-CONICET, Bahía Blanca, Argentina*
[c] *Department of Chemistry, University of Aveiro, CICECO, 3810-193 Aveiro, Portugal*

Received 15 November 2005; received in revised form 15 February 2006; accepted 5 March 2006
Available online 17 March 2006

Abstract

MCM-48 membranes have been prepared on alumina supports of different pore sizes. A battery of characterization techniques has been used to study the physical properties and the quality of the membranes prepared. The highest quality membranes were prepared on supports with pore size of up to 60 nm. The MCM-48 membranes were tested in the separation of gas phase mixtures and a cyclohexane/O_2 selectivity higher than 270 was obtained. The selective separation of organic compounds from inert components is a result of the cooperative effects of capillary condensation in MCM-48 pores and of the specific interactions of the permeating compounds and the membrane material.

Keywords: Mesoporous membranes; MCM-48; zeolite membranes; organic/permanent gas separation

1. Introduction

Microporous inorganic membranes have been extensively studied during the last decade as an alternative to polymeric membranes. Among them, zeolite membranes show great potential for applications as membrane separators, membrane reactors and sensing devices due to their diversity of structures and thermal and chemical stability. Nevertheless, zeolite structures have pores of subnanometric size, which imposes a limit on the size of molecules that can be processed. Therefore, when relatively large molecules are to be separated, other types of porous membranes must be used.

Mesoporous inorganic membranes have also been investigated, mainly consisting of silica, titania, and zirconia, often prepared by the sol–gel method. These membranes are amorphous and do not posses an ordered structure. A different kind of material is the so-called M41S [1,2], whose surfactant-mediated synthesis was first reported in 1992 by researchers from Mobil Oil Corporation. Among M41S are MCM-41 and MCM-48 with uniform pore structures of hexagonal and cubic symmetry, respectively. These materials are interesting for the preparation of membranes as they present narrow pore size distributions that can be tuned from 2 to10 nm.

The preparation of films of these materials has been accomplished primarily over non-porous substrates (e.g., mica [3], glass [4,5], silicon wafers [6,7]), which are not suitable as membrane supports. The first attempt to grow mesostructured silica films on a support was reported in 1996 by Yang et al. [3], who carried out the hydrothermal treatment of a mica support immersed in an aqueous-acid-surfactant mixture. As an alternative synthesis procedure, a classical sol–gel route has been employed for the preparation of the precursor containing the hydrolyzed silica source and the surfactant, followed by deposition of the sol on the support (dip-coating or spin coating) and solvent evaporation. Using this method Ogawa and Masukawa [5] prepared thin films of lamellar, hexagonal and cubic mesoporous silica, over pyrex glass substrates.

While these studies are useful to investigate the conditions leading to the growth of mesostructured films, the application of these films as membranes requires synthesis over porous supports that enable permeation of the target molecules. A further issue to take into account concerns the alignment of the membrane pores with regards to the support surface. While this is not a problem when the three-dimensional structure of MCM-48 is used, alignment of the pore network of MCM-41 parallel to the support surface hinders permeation. This has led to attempts to attain perpendicular alignment of the pores with respect to the

* Corresponding author. Tel.: +34 976 761153; fax: +34 976 762142.
E-mail address: iqcatal@unizar.es (J. Santamaría).

0376-7388/$ – see front matter © 2006 Elsevier B.V. All rights reserved.
doi:10.1016/j.memsci.2006.03.016

support surface, often by unusual procedures (e.g. magnetic field alignment [8]).

Nishiyama et al. [9], using a hydrothermal treatment, were able to present the first gas-permeable mesoporous silica membranes made of MCM-48. These membranes were synthesized over flat porous stainless steel supports that were placed horizontally in the autoclave containing the sol precursor during at least two days. The same group [10] presented permeance measurements of different gases and carried out a permeance versus pressure study that confirmed a Knudsen permeation mechanism for these membranes, with nitrogen permeances around $2.5\,10^{-7}$ mol/m^2 s Pa. EDX analysis showed that the membrane consisted of a layer prepared on top of the support, with some siliceous material penetrating the support pores. In a separate study of the same laboratory [11], silylation was carried out using trimethylchlorosilane and triethylclorosilane as silylation reagents, in order to enhance the hydrophobicity and hydrothermal stability of these membranes. The silylated MCM-48 membranes where used for the separation of organic/water mixtures, the organic component being ethanol, methyl-ethyl-ketone or ethyl acetate. They found separation factors and organic permeation fluxes as high as 320 and 5.8 kg/m^2 h, respectively, for a mixture containing 5% of ethyl acetate in water at 300 K.

The synthesis over porous supports, using the sol–gel technique has been less studied. 'Kim and Yang [12] used this method to prepare thin films of mesoporous silica with a cubic structure over α-alumina porous supports whose pores had previously been filled with PVA to prevent sol penetration. This produced 1 μm thick films. However, no permeation measurements were reported.

McCool et al. [13] synthesised mesoporous silica membranes over flat α-alumina supports using both dip-coating and hydrothermal treatment as synthesis methods. While both types of preparation methods yielded membranes that exhibited Knudsen permeation, the fluxes for the dip-coated membrane were nearly three times higher. The maximum separation factor for N_2/Ar mixtures was 1.35 and 1.2 for the hydrothermal-treated and dip-coated membranes, respectively. Mesoporous silica membranes have also been synthesised on flat alumina supports for filtration applications [14] and solvent permeation [15] using the dip-coating and spin-coating techniques.

To our knowledge, the synthesis of MCM-48 membranes over tubular supports has only been reported by Liu et al. [16] but no separation results were presented. The aim of the present work is to contribute to the study of MCM-48 membranes on tubular supports, which are those better suited for industrial use. To this end, we present the preparation of these membranes using hydrothermal synthesis, as well as data obtained from characterization experiments by a battery of techniques: XRD, BET specific surface area, SEM, FTIR, single-gas permeation and permporometry. The MCM-48 membranes were also tested in the gas phase separation of mixtures containing an adsorbable organic compound and an inert component.

2. Experimental

2.1. Synthesis of the membranes

The membranes were prepared on tubular asymmetric supports (Inocermic) of 7 mm i.d., 10 mm o.d. At the innermost part of these ceramic tubes there is either a γ-Al_2O_3 layer, with pores of 5 or 60 nm, or a α-Al_2O_3 layer with 200 nm pores. In order to confine the permeation zone, the supports were subjected to enameling at both ends, defining a permeation length of approximately 5 cm.

The precursor gel for the MCM-48 synthesis had the following molar composition: 1 SiO_2: 61.44 H_2O: 0.62 CTMACl: 0.5 NaOH [17]. In a typical synthesis, TEOS (tetraethylorthosilicate) was added to a sodium hydroxide solution with stirring for 5 min to form a clear solution. Afterwards, surfactant, cetyltrimethylammonium chloride, CTMACl, was added. The mixture was maintained under stirring for 15 min more and the solution turned into a white gel. The gel was then introduced into the pores of the support by immersing the membrane tube into a vessel containing the gel and applying vacuum to its inner side. The gel-containing support was then introduced in a Teflon-lined autoclave containing the synthesis gel, and subjected to hydrothermal treatment in vertical (static) or horizontal (rotatory) position, for 48 h at 363, 376 or 383 K. The synthesis produced MCM-48 on the membrane, and also as a powder which could be collected at the bottom of the autoclave after reaction. The powder product and the membrane were washed with distilled water and dried at room temperature overnight. The material gain of the membrane (see Table 2) was calculated as the weight difference between the membrane after synthesis and the initial support.

The synthesis procedure was repeated until the N_2 permeance became null, usually taken as an indication of good membrane quality. The removal of the surfactant was carried out either by calcination or solvent extraction. A two-step procedure was adopted for the calcinations, with a first stage of heating under N_2 flow (200 N mL/min) at 2 K/min to 813 K, followed by 6 h under air (200 N mL/min) at this temperature. For the chemical extraction, a solution containing EtOH and HCl was used at 328 K for 8 h under reflux. For this procedure, each gram of MCM-48 was refluxed with 7 g of HCl (37 wt.%) and 250 mL of pure ethanol.

2.2. Characterization

The structure of materials obtained after synthesis was characterized by X-ray diffraction (XRD) (Cu Kα radiation on a Philips X'pert MPD). The BET surface area and pore size distribution of the powder were obtained by N_2 adsorption measurements on a Micromeritics ASAP 2020. The morphology of membranes was characterized by scanning electron microscopy (SEM, JEOL JSM-6400 operating at 20 kV). Infrared spectroscopy was used for the examination of MCM-48 samples after removal of the surfactant by different methods. The FTIR spectra were collected with a Mattson Research Series II instrument, equipped with a MCT detector (DRIFT

analysis, at 4 cm^{-1} resolution and with a collection speed of 300 scans/min).

Further characterization of the quality of the MCM-48 membranes was carried out by single gas permeation measurements (N_2) and by permporometry. The latter technique involves measuring the flux of a non-condensable gas under conditions where capillary condensation of water or organic vapours occurs. This method was employed to characterize the pore size distribution of the membrane.

2.3. Separation of mixtures

The membranes were tested for cyclohexane/O_2 gas separation. The gas mixture was fed into the tube side of the membrane (retentate) and an inert sweep gas (He) was used on the permeate side. The gaseous mixture was obtained by bubbling an O_2 stream through a saturator containing cyclohexane at a known temperature. Experiments were carried out with a feed containing around 10% of cyclohexane by volume, with feed and sweep gas flow rates ranging from 50 to 200 N mL/min. The experiments were carried out at room temperature and the pressure on both sides of the membrane was maintained at atmospheric pressure (101 kPa). When steady state was reached, samples at the exit of both the tube and the shell side were analyzed by on-line gas chromatography (HP 5890 SERIES II).

The permeation fluxes P, and the separation selectivity S were calculated by the following expressions:

$$S_{(\text{organic}/O_2)} = \frac{P_{\text{organic}}}{P_{O_2}}$$

$$P_i = \frac{F_p y_{i,p}}{S_p \Delta P_{\log,i}}$$

where S is the selectivity, P_i the permeance of component i, y_{ip} the molar fraction of component on the permeate side, S_p the permeable membrane area, ΔP the log-mean partial pressure drop, and F_p the molar flow at the permeate side.

3. Results and discussion

3.1. Characterization of powders

In order to select appropriate conditions for membrane synthesis, some preliminary experiments were carried out in which MCM-48 samples were prepared as powder, using different temperatures and synthesis times. The XRD patterns corresponding to the samples prepared as powder are presented in Fig. 1. In agreement with the results of Beck et al. [1], it can be seen that the samples synthesized at 363 and 373 K display MCM-50 and MCM-41 structures, while the patterns corresponding to the samples prepared at 383 K reveal the desired 3D cubic MCM-48 structure, irrespective of whether the synthesis was carried out in two or four days. Therefore, a synthesis time of two days and a temperature of 383 K were selected for the synthesis of MCM-48 membranes. In Fig. 1b, the diffraction patterns corresponding to the samples after calcination are shown. It can be seen that the structure is maintained, and all the peaks remain present after removal of the surfactant; however a displacement to higher 2θ values is observed for the calcined sample, indicating a decrease in the d space of the structure. This effect could be attributed to shrinkage of the structure as a consequence of surfactant removal. The shrinkage translates into a decrease of ca. 15% in the d (2 1 1) values after surfactant removal, from 39.8 Å for the *as prepared* sample.

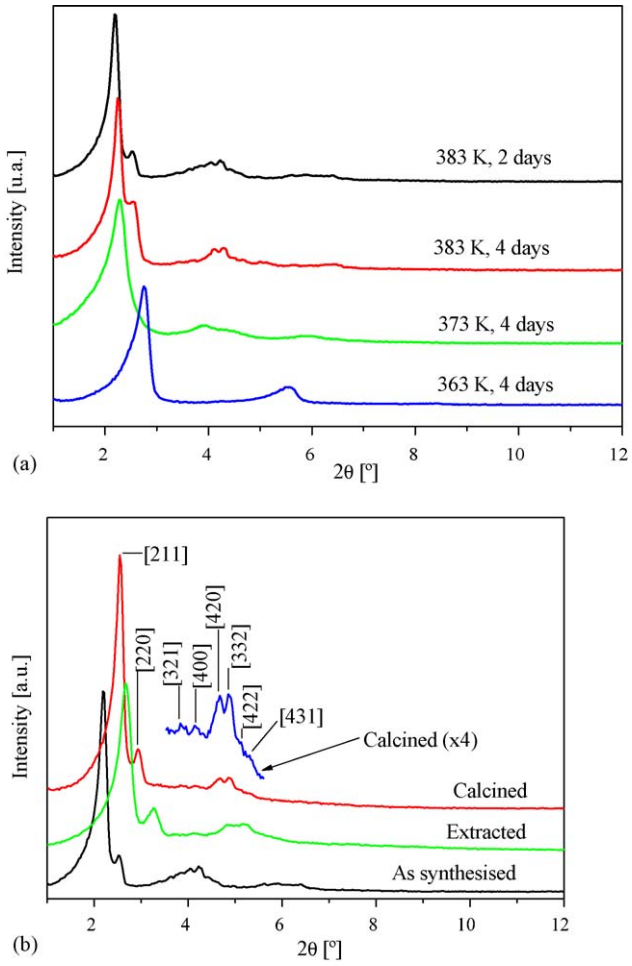

Fig. 1. (a) Diffraction patterns of the powders synthesized under different conditions. (b) Diffraction patterns of the MCM-48 material as synthesized (2 days, 383 K), and after removal of the surfactant by solvent extraction or calcination.

Table 1 shows the results of N_2 adsorption experiments for MCM-48 powder samples that differ in the method of template removal (calcination or solvent extraction). While the specific BET surface area is high in both cases, it can be seen that the values for the extracted sample are smaller, and the same can be said of the measured pore volume; this could be attributed to the

Table 1
Structural parameters obtained from N_2 adsorption isotherms after surfactant removal by calcination and solvent extraction

Parameter	Calcination	Solvent extraction
BET specific surface area (m^2/g)	762	631
Pore volume (cm^3/g)	0.790	0.609
Average pore diameter (nm)	3.15	2.95

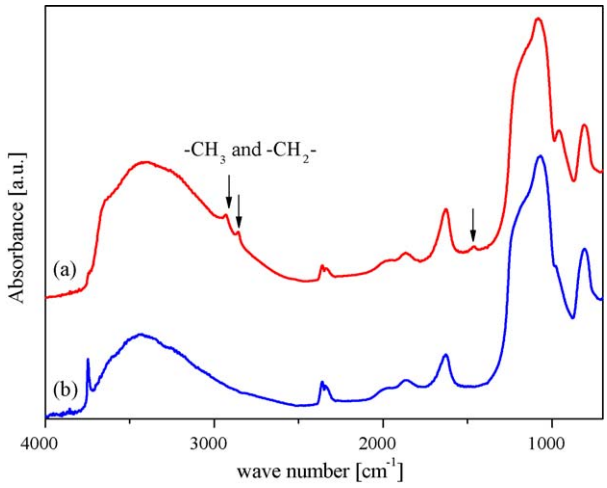

Fig. 2. DRIFT spectra for MCM-48 samples in which the surfactant had been removed by: (a) extraction; (b) calcination.

fact that calcination is more efficient for removing the surfactant compared to the extraction process. In the same way, the small difference observed for the mean pore size could be explained by assuming that a fraction of the surfactant still remains inside the pore structure for the extracted sample. Direct evidence of this presence was obtained from the DRIFT measurements shown in Fig. 2. As can be observed, some absorbance peaks corresponding to alkyl stretching can still be appreciated in the sample subjected to surfactant removal by extraction (Fig. 2, curve a), while they were absent from the calcined sample.

3.2. Characterization of membranes

Table 2 lists the synthesis conditions and some basic characteristics of the membranes prepared in this work. It can be observed that the membranes prepared on supports with smaller pore diameters showed in general lower N_2 permeances, suggesting that these membranes have a lower concentration of inter-crystalline defects. In fact, while the permeances span two orders of magnitude, the weight gains obtained for the different membranes are within a relatively narrow range (a factor of 2), suggesting similar effective thicknesses of the membrane material. Therefore, differences in membrane quality, rather than membrane thickness, seem the most likely explanation for the differences in permeance observed.

An examination of the values of the Knudsen contribution to the permeation flux given in Table 2 also confirms this assertion. For weakly or non-interacting gases (such as N_2), the permeance through a porous membrane can be expressed as [18]:

$$F = \alpha + \beta P_{av}$$

where F is the permeation flux per unit of time, area and transmembrane pressure difference (mole/m^2 sbar), P_{av} the average pressure across the membrane (bar), and α and β indicate, respectively, the Knudsen and laminar contributions to the permeation flux. In this way, the representation of permeance against the mean pressure (Fig. 3) results in a straight line where the intercept value (α) is related to the Knudsen contribution and the slope (β) to the viscous flow. From these two values the percentage contribution of the Knudsen flow to the total flow (at P_{av} equal to 1 bar) can be obtained, and is given in Table 2 for each of the membranes prepared. Since viscous flow is related to the presence of relatively large inter-crystalline defects, a low value of the viscous contribution (a high value of the Knudsen percentage) can be taken as a reliable indication of membrane quality. Fig. 3 illustrates the dependence of the N_2 permeance with the mean pressure for four different membranes used in this work. It can be observed that the line representing membrane M-1 (prepared on a support with 1900 nm pores) has a steep slope, indicating a high contribution of the viscous flow (36.2%, i.e.,

Table 2
Synthesis conditions and some relevant characteristics of the membranes prepared in this work

Membrane	Support	Synthesis method	Surfactant removal	Gain (mg/g)	N_2 permeance (mol/(m^2 s Pa))	% Knudsen
M-1[a]	α-1900	Static	Calcination	9.0	3.51×10^{-6}	63.8
M-2[a]	α-1900	Static	Calcination	12.5	5.71×10^{-6}	58.2
M-3[a]	α-200	Static	Calcination	13.2	9.70×10^{-7}	92.6
M-4[a]	α-200	Static	Calcination	10.2	1.10×10^{-6}	98.6
M-5[a]	α-200	Static	Calcination	10.9	1.04×10^{-6}	95.9
M-6	α-200	Rotatory	Extraction	9.3	1.39×10^{-6}	86.7
M-7	γ-60	Static	Calcination	7.3	2.24×10^{-6}	83.8
M-8	γ-60	Rotatory	Calcination	10.7	2.50×10^{-6}	98.1
M-9	γ-60	Rotatory	Extraction	9.0	9.16×10^{-7}	99.0
M-10	γ-60	Rotatory	Extraction	9.8	8.54×10^{-7}	99.2
M-11[a]	γ-60	Rotatory	Extraction	12.3	2.42×10^{-7}	90.4
M-12	γ-5	Static	Calcination	6.7	1.08×10^{-6}	70.8
M-13	γ-5	Rotatory	Calcination	10.3	3.68×10^{-6}	73.6
M-14	γ-5	Rotatory	Extraction	11.6	2.93×10^{-8}	99.0
M-15	γ-5	Rotatory	Extraction	9.9	7.53×10^{-9}	97.4
M-16	γ-5	Rotatory	Extraction	10.3	1.45×10^{-8}	94.1
M-17	γ-5	Rotatory	Extraction	13.2	1.63×10^{-8}	89.8
M-18	γ-5	Rotatory	Extraction	12.5	7.90×10^{-9}	99.0

[a] Two syntheses.

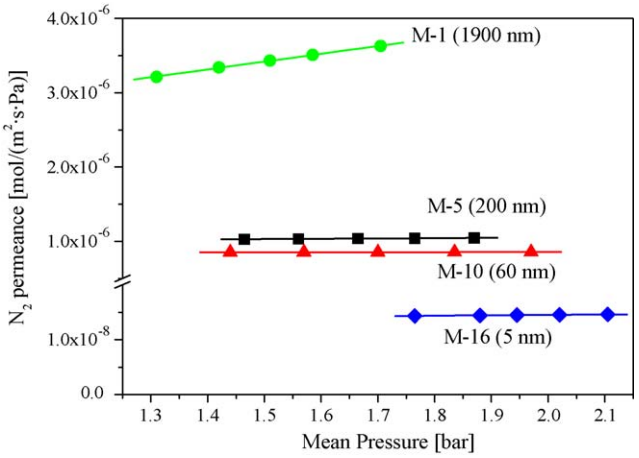

Fig. 3. N_2 permeance vs. average pressure for several MCM-48 membranes.

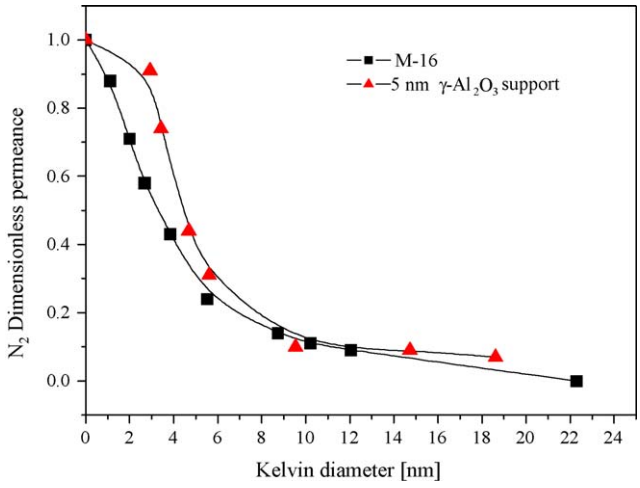

Fig. 4. Dimensionless permeance as a function of Kelvin diameter for membrane M-16 and for a 5 nm γ-Al_2O_3 tubular support.

a Knudsen contribution of only 63.8%). On the other hand the lines corresponding to membranes M-5, 10 and 16 (prepared on supports with pore sizes up to 200 nm) are almost horizontal, and their Knudsen contributions are accordingly higher (95.9; 99.2 and 94.1%, respectively).

When comparing the Knudsen contributions given in Table 2 for membranes where surfactant removal was carried out by different methods, it is interesting to note that the Knudsen contribution is significantly higher in the membranes treated by extraction. Thus, the average values of Knudsen contribution (membranes prepared on supports of 5, 60 and 200 nm), were 87.6% and 94.9% for calcined and extracted membranes, respectively, indicating a higher quality for the extracted membranes. This conclusion is also supported by the separation results: of the membranes in Table 2, the 7 highest values of separation selectivity were obtained with membranes treated by extraction. This suggests the formation of pinholes or cracks during surfactant removal by calcination, in part as a consequence of the thermal stresses produced in the process.

Finally, an estimation of the size of defects and their contribution to the permeation flux can also be obtained using permporometry, a non-destructive characterization technique that yields information on the distribution of fluxes through those pores that are active for permeation in a given membrane [19]. We have used water vapour/N_2 streams on the feed side of the membrane, and measured the permeation of N_2 at different partial pressures of water vapour. Since capillary condensation at a given partial pressure can be related to the pore radius by the Kelvin equation, the permeation flux as a function of pore radius can be obtained. Fig. 4 displays the dimensionless permeance of N_2 (defined as the ratio of N_2 permeance at a certain concentration of water vapour to the N_2 permeance in the absence of capillary condensation) as a function of the Kelvin diameter for membrane M-16 (94.1% of Knudsen contribution). For comparison, the same curve for an untreated γ-Al_2O_3 support with 5 nm pores is also presented.

Fig. 4 is in fact a plot of cumulative permeance through pores larger than a certain size. Therefore, if we define the mean pore diameter for permeation [19] as the pore diameter corresponding to 50% of the total permeance, it can be observed that a value of approximately 5 nm is obtained for the γ-Al_2O_3 support, which is in agreement with the manufacturer's data. On the other hand, the mean pore diameter obtained for membrane M-16 was 3.35 nm, which is close to the value obtained from the N_2 adsorption data for MCM-48 powder (2.95–3.15 nm, see Table 1). The proximity of these two values again indicates a good quality for this membrane (which is in agreement with its relatively high Knudsen contribution), since the presence of large inter-crystalline defects would translate into a considerable difference between the average pore diameter for the membrane and the characteristic pore diameter of the constituting material. However, the permporometry plot also indicates that, in spite of the good overall quality of the membrane, around 10% of the permeation flux still occurs through pores of 12 nm and larger.

Fig. 5 shows SEM micrographs corresponding to different views of membrane M-17, synthesized on a 5 nm support. In both the external and internal surface, silica spheres corresponding to MCM-48 material can be observed. Fig. 4(e) and (f) shows the cross sections of the MCM-48 films grown respectively on the external and internal surfaces of the tubular support. While in both cases a continuous layer can be observed, the outside film is thicker (9 μm, compared to 3 μm for the inner-side film). This is a consequence of the method of introduction used for the synthesis gel, which is suctioned inwards through the membrane outer surface.

3.3. Separation of cyclohexane/oxygen mixtures

The experiments for the separation of mixtures were carried out with membrane M-18, in principle the membrane with the lowest concentration of defects in Table 2, in view of its low N_2 permeance and high Knudsen contribution. A cyclohexane/O_2 mixture was introduced in the membrane feed side at room temperature as an example of a separation involving adsorbable/inert components, under variable conditions of feed-side and sweep gas flow, and cyclohexane concentration.

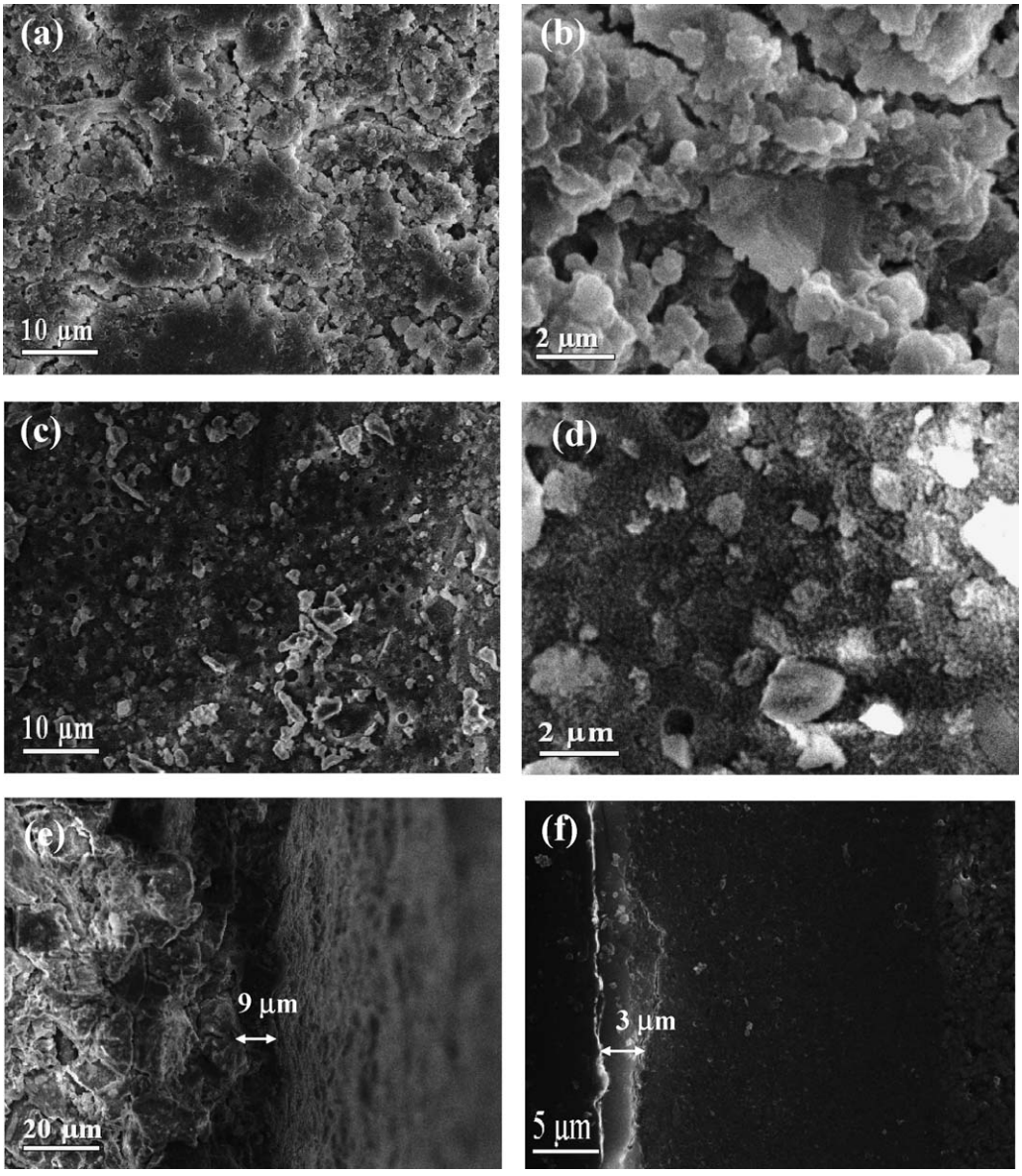

Fig. 5. SEM micrographs of membrane M-17: (a) and (b) top view external surface; (c) and (d) top view of the internal surface; (e) external cross-section; (f) internal cross-section.

Fig. 6 shows the effect of feed-side flow on the cyclohexane/O_2 separation selectivity. It can be seen that both the selectivity and the cyclohexane permeance increase with the feed flow. The selectivity reaches a value of 276 for a feed flow of 150 N mL/min, and from this point stays at an approximately constant level. This is a consequence of the higher effective cyclohexane concentrations that are reached at the feed side for increasing values of the feed flow. For a low feed flow rate, a significant proportion of the cyclohexane in the feed permeates, thereby decreasing the average cyclohexane concentration in the feed side. On the other hand, as the feed flow increases, the cyclohexane concentration at the exit of the retentate also increases, becoming closer to the feed concentration value. Since the separation selectivity depends on the successful blocking of O_2 permeation by adsorbed and/or condensed cyclohexane, an increase of cyclohexane concentration not only increases the

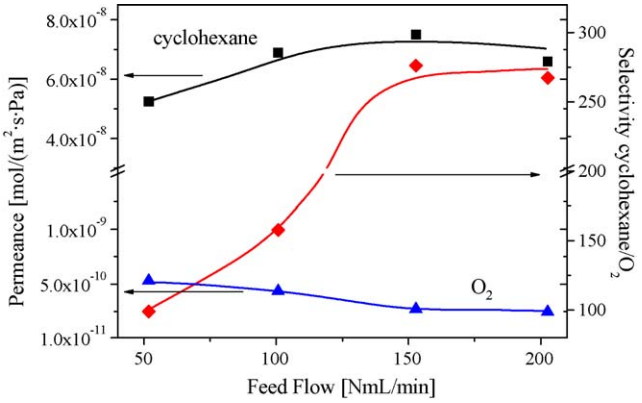

Fig. 6. Permeance and selectivity vs. feed flow for membrane M-18. Room temperature; sweep gas flow rate: 50 mL(STP)/min; cyclohexane concentration in the feed 10%.

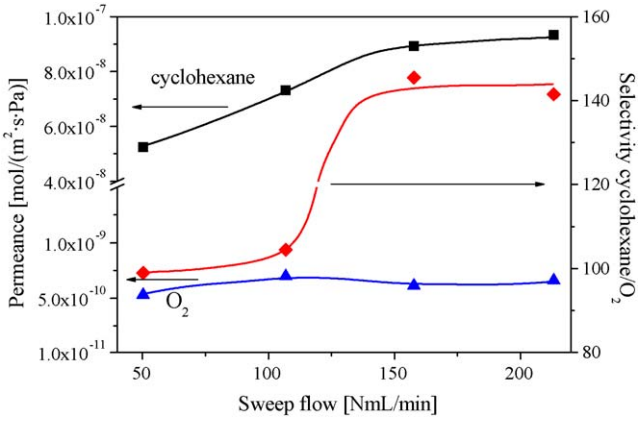

Fig. 7. Selectivity and permeance as a function of sweep gas flow rate for membrane M-18. Room temperature; feed flow rate: 50 mL(STP)/min; cyclohexane concentration in the feed was 11.5%.

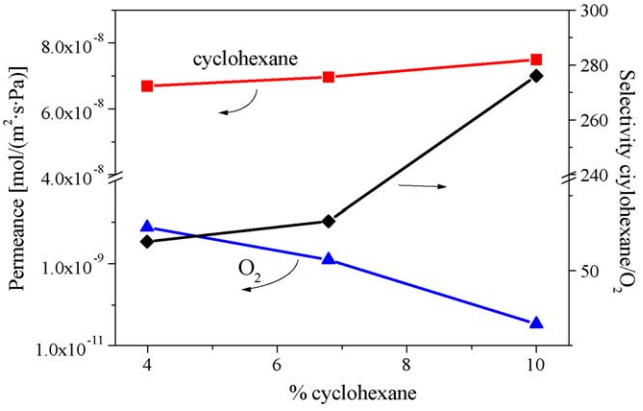

Fig. 8. Permeances of cyclohexane and oxygen and separation selectivity vs. concentration of cyclohexane in the feed for membrane M-18. Room temperature; feed flow rate: 150 mL(STP)/min; sweep gas flow rate: 50 mL(STP)/min.

driving force for cyclohexane permeation, but also makes more effective the blocking effect, as can be seen from the decrease of O_2 permeance.

The effect of the sweep gas flow rate is presented in Fig. 7 for a fixed cyclohexane concentration and feed flow rate. It can be seen that the cyclohexane/O_2 selectivity increases with the sweep gas flow rate until again a roughly constant value (146 in this case) is reached at a flow rate of 150 N mL/min. It can also be observed that the selectivity increase is a consequence of the marked increase in cyclohexane permeance with the sweep gas flow rate, while the effect on O_2 permeance is much lower. This can be explained by the increase in the driving force for permeation that takes place as the sweep gas flow rate increases, and the partial pressure of cyclohexane in the permeate side decreases accordingly. This effect is less pronounced than for the case of the feed flow rate, since the partial pressure of cyclohexane at the permeate side is already low, but is nevertheless significant. The effect on O_2 permeation is only minor, as the access of this molecule to the membrane pores is hindered by adsorbed cyclohexane.

Fig. 8 shows the results obtained when the concentration of cyclohexane in the feed was increased, while keeping constant other operating conditions. A steep increase in selectivity can be observed, which in this case is not originated by a corresponding increase in the cyclohexane permeance (which increases only moderately), but by a strong decrease in the O_2 permeance. This indicates that cyclohexane molecules in the MCM-48 pore system are able to block the pass of O_2 with a higher efficiency as cyclohexane concentration increases. This is at least in part a consequence of the capillary condensation of cyclohexane in the pores of MCM-48, which takes place at the concentrations used. However, the preferential adsorption of cyclohexane also seems to play a significant role in the separation observed, as will be shown next.

The Kelvin radius has been calculated for each concentration used in the experiment of Fig. 8, and is given in Table 3. At the higher partial pressures used ($P/P_0 = 0.62$ and 0.41) the Kelvin diameter for the mixture is higher than the mean pore diameter of the MCM-48 material given in Table 1, i.e. cyclohexane should condense in the MCM-48 pores, and also in those inter-crystalline defects that are smaller than the corresponding Kelvin diameter. However, as Fig. 4 indicates, there are pores which are larger than any of the calculated Kelvin diameters and cannot be blocked by condensed cyclohexane. In spite of this, high selectivity values are obtained (276 for 8.5% cyclohexane in the feed). Also, a good selectivity (60) is obtained for 4% cyclohexane in the feed, when the Kelvin diameter is below the MCM-48 pore size. This value of selectivity can be compared to the value of only 11.5 obtained with a γ-Al_2O_3 support, in spite of the fact that the calculated Kelvin diameter for the mixture (8.9 nm) is much higher than the mean pore diameter of the support evaluated by permporometry (4.5 nm).

These observations suggest that capillary condensation alone cannot explain the separation observed with the MCM-48 membranes, and specific interactions between cyclohexane and the MCM-48 material must be taken into account. Further support for this explanation was obtained from the fact that, when, in a separate experiment, the temperature was raised to 408 K, under a concentration of 10% cyclohexane in the feed a selectivity of

Table 3
Selectivity cyclohexane/O_2 and Kelvin diameter for the experiments in Fig. 8 and an experiment with a γ-Al_2O_3 support

Membrane	% Cyclohexane in the feed/temperature (K)	P/P_0	Kelvin diameter (nm)	Selectivity cyclohexane/O_2
M-18	8.5/299	0.62	8.7	276
	6.8/303	0.41	4.5	66
	4.0/303	0.24	2.8	60
γ-Al_2O_3 support (5 nm pores)	9.1/299	0.63	8.9	11.5

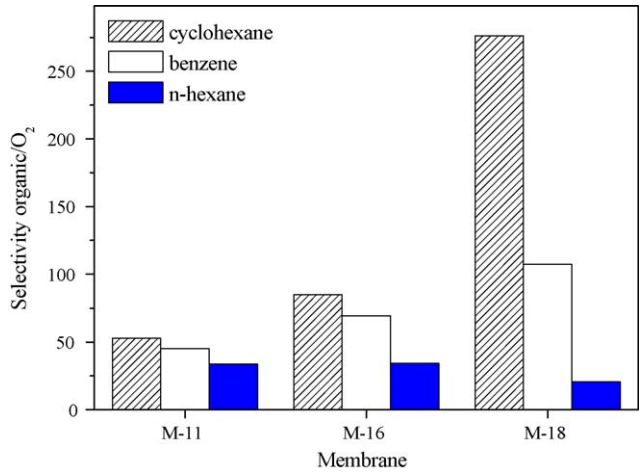

Fig. 9. Selectivity of the organic/O_2 separation for different MCM-48 membranes. Room temperature; feed flow rate: 150 mL(STP)/min; sweep gas flow rate: 100 mL(STP)/min; except for membrane M-18 (sweep gas flow rate: 50 mL(STP)/min). Organic concentrations: cyclohexane, 10%; benzene, 6%; *n*-hexane, 14%.

10 was still obtained (the Knudsen value is 1.6), in spite of the fact that under these conditions capillary condensation cannot take place.

3.4. Separation of different organic compounds

In addition to the separation of cyclohexane/O_2 mixtures already discussed, the separation of benzene/O_2 and *n*-hexane/O_2 mixtures was also carried out. In each case, the concentration of the organic component in the feed was obtained by passing an O_2 stream through a bubbler containing the organic compound. This yielded 10% for cyclohexane, 6% for benzene and 14% for *n*-hexane. Fig. 9 shows the organic/O_2 selectivity obtained at 298 K with these compounds on three different membranes. It can be seen that the selectivity obtained with *n*-hexane was the lowest in all cases, in spite of the higher concentration used in this case, while that obtained with cyclohexane was the highest. The separation selectivity observed can be related to the differences in the adsorption of these compounds on MCM-48. Zhao et al. [20] studied the adsorption characteristics of these three compounds over a MCM-41 sample using a temperature-programmed desorption technique and found that the activation energies for desorption followed the order cyclohexane ≈ benzene > *n*-hexane. A similar behaviour over MCM-48 can reasonably be expected, thus explaining the higher selectivity obtained with cyclohexane and benzene. A further parameter can be considered here, related to the size of the molecules and how they adsorb in the pores, since this will affect the blocking of oxygen permeation. Cyclohexane and benzene are bulkier than *n*-hexane (kinetic diameters of 6, 5.85 and 4.3 Å, respectively), and therefore can be expected to be more effective at pore blocking, which is in agreement with the selectivities shown in Fig. 9. In addition, the electronic cloud over the benzene ring is likely to interact with the silanol groups at the MCM-48 surface, further increasing its effectiveness for blocking. This may explain the efficient blockage obtained with benzene, in spite of a concentration of only 6% in the feed. Finally, hexane not only adsorbs less, but also has a smaller kinetic diameter and can be adsorbed in parallel to the pore wall, leaving enough space for the permeation of O_2, thus reducing its blocking capacity, in agreement with the results of Fig. 9.

4. Conclusions

The synthesis of mesoporous MCM-48 membranes on alumina supports has been successfully accomplished. The MCM-48 deposits formed as a layer on top of the supports, and also partially inside the support pores. Organic compounds were selectively separated from inert components as a result of the cooperative effects of capillary condensation in the membrane pores and of the specific interactions of the organic species and the MCM-48 material. These mechanisms yielded selectivities that reached values in excess of 270 for the separation of cyclohexane/oxygen mixtures.

The method of surfactant removal played a key role on the characteristics of the membranes prepared: while calcination was more efficient in removing the surfactant, extraction preserved better the integrity of the MCM-48 films, resulting in membranes of a higher quality. The size of the support pores also had a significant influence on membrane quality, with the best performing membranes prepared on supports with pores of 60 nm and lower.

Acknowledgements

Financial support from DGA and MEC, Spain, is gratefully acknowledged.

References

[1] J.S. Beck, J.C. Vartulli, W.J. Roth, A new family of mesoporous molecular-sieves prepared with liquid-crystal templates, J. Am. Chem. Soc. 114 (1992) 10834.
[2] C.T. Kresge, M.E. Leonowicz, W.J. Roth, J.C. Vartulli, J.S. Beck, Ordered mesoporous molecular sieves synthesized by a liquid-crystal template mechanism, Nature 359 (1992) 710.
[3] H. Yang, A. Kuperman, N. Coombs, S. Mamiche-Afara, G.A. Ozin, Synthesis of oriented films of mesoporous silica on mica, Nature 379 (1996) 703.
[4] M. Ogawa, H. Ishikawa, T. Kikuchi, Preparation of transparent mesoporous silica films by a rapid solvent evaporation method, J. Mater. Chem. 8 (1998) 1783.
[5] M. Ogawa, N. Masukawa, Preparation of transparent thin films of lamellar, hexagonal and cubic silica-surfactant mesostructured materials by rapid solvent evaporation methods, Micropor. Mesopor. Mater. 38 (2000) 35.
[6] Y.F. Yf, R. Ganguli, C.A. Drewien, M.T. Anderson, C.J. Brinker, W.L. Gong, Y.X. Guo, H. Soyez, B. Dunn, M.H. Huang, J.I. Zink, Continuous formation of supported cubic and hexagonal mesoporous films by sol gel dip-coating, Nature 389 (1997) 364.
[7] D. Zhao, P. Yang, N. Melosh, J. Feng, B.F. Chmelka, G.D. Stucky, Continuous mesoporous silica films with highly ordered large pore structures, Adv. Mater. 10 (1998) 1380.
[8] S.H. Tolbert, A. Firouzi, G.D. Stucky, B.F. Chmelka, Magnetic field alignment of ordered silicate-surfactant composites and mesoporous silica, Science 278 (1997) 264.

[9] N. Nishiyama, A. Koide, Y. Egashira, K. Ueyama, Mesoporous MCM-48 membrane synthesized on a porous stainless steel support, Chem. Commun. (1998) 2147.
[10] N. Nishiyama, D.H. Park, A. Koide, Y. Egashira, K. Ueyama, A mesoporous silica (MCM-48) membrane: preparation and characterization, J. Membr. Sci. 182 (2001) 235.
[11] D.H. Park, N. Nishiyama, Y. Egashira, K. Ueyama, Separation of organic/water mixtures with silylated MCM-48 silica membranes, Micropor. Mesopor. Mater. 66 (2003) 69.
[12] Y.-S. Kim, S.-M. Yang, Preparation of continuous mesoporous silica thin film on a porous tube, Adv. Mater. 14 (2002) 1078.
[13] B.A. McCool, N. Hill, J. Di Carlo, W.J. DeSisto, Synthesis and characterization of mesoporous silica membranes via dip-coating and hydrothermal deposition techniques, J. Membr. Sci. 218 (2003) 55.
[14] K. Nakagawa, M. Matsuyama, T. Maki, M. Teramoto, N. Kubota, Preparation of mesoporous silica membrane by solvent evaporation method for filtration application, Sep. Purif. Technol. 44 (2005) 145.
[15] S.R. Chowdhury, R. Schmuhl, K. Keizer, J.E. ten Elshof, D.H.E. Blank, Pore size and surface chemistry effects on the transport through mesoporous g-alumina and silica MCM-48, J. Membr. Sci. 225 (2003) 177.
[16] C. Liu, Y. Wang, H. Tong, Synthesis and characterization of mesoporous silica (MCM-48) membrane on a porous ceramic tube, in: Proceedings of the International Conference on Inorganic Membranes (ICIM 8), Cincinnati, OH, July 18–22, 2004, pp. 34–37.
[17] J. Xu, Z. Luan, H. He, W. Zhou, L. Kevan, A reliable synthesis of cubic mesoporous MCM-48 molecular sieve, Chem. Mater. 10 (1998) 3690.
[18] Y.S. Lin, A.J. Burggraaf, Preparation and characterization of high-temperature thermally stable alumina composite membrane, J. Am. Ceram. Soc. 74 (1991) 219.
[19] T. Tsuru, T. Hino, T. Yoshioka, M. Asaeda, Permporometry characterization of microporous ceramic membranes, J. Membr. Sci. 186 (2001) 257.
[20] X.S. Zhao, G.Q. Lu, X. Hu, Organophilicity of MCM-41 adsorbents studied by adsorption and temperature-programmed desorption, Colloid. Surf. A 179 (2001) 261.